PERGAMON

International Journal of Solids and Structures 40 (2003) 5319–5334

INTERNATIONAL JOURNAL OF SOLIDS and STRUCTURES

www.elsevier.com/locate/ijsolstr

Design enhancements for stress relaxation in automotive multi-shell-structures

Hyungyil Lee [a,*], Heon Seo [b], Gyung-Jin Park [c]

[a] *Department of Mechanical Engineering, Sogang University, MapoGu, SinsuDong 1, Seoul 121–742, South Korea*
[b] *Auto Frame Design Group, Kia Motor Company, KyungGi 445–706, South Korea*
[c] *Department of Mechanical Engineering, Hanyang University, KyungGi 426–791, South Korea*

Received 11 November 2002; received in revised form 9 May 2003

Abstract

Recent attempt to enhance the safety against collision has reshaped the simple single-shell structure into the integrated multi-shell structure. Moreover, due to various regulations continuously tightened for environment, weight reduction of automobile becomes an increasingly important issue. Weight reduction is mainly accomplished by better redesign, adoption of lighter materials, and small-sizing of auto (parts). Focusing on the local redesign among three, we suggest local patching methods. We also present, as another way, a method of determining thicknesses of subpart-shells in an integrated multi-shell structure. Those redesign methods successfully bring a preset amount of stress relaxation. More specifically, we first select a cross member as local patching model. Based on the finite element stress calculations, we relieve the stress of cross member by patching in two ways—non-uniform thickness patching and optimized uniform thickness patching. The latter is more effective and practical. Selecting a box type subframe as other redesign model, we determine the thickness of each subpart-shell by axiomatic design approach. The patching methods and the axiomatic approach of this work can be extended to the other multi-shell structures such as center member and lower control arm.

Keywords: Multi-shell-structure; Cross member; Subframe; Finite element method; Patch; Stress relaxation; Optimization, Axiomatic design

1. Introduction

Safety during a car crash takes recent worldwide concern. Especially in Europe and USA, safety regulations are constantly strengthened, which leads automotive manufacturers to make various endeavors for the guarantee of the safety of the passenger (Lam, 2003; Hong and Park, 2003; Ambrosio, 2003). Consequently, the technology level for the design of a safe auto-body becomes a main measure of international competitiveness of an auto manufacturer. This trend has changed some front parts of an auto-body from a

* Corresponding author. Tel.: +82-2-705-8636; fax: +82-2-712-0799.
E-mail address: hylee@sogang.ac.kr (H. Lee).

0020-7683/$ - see front matter © 2003 Elsevier Ltd. All rights reserved.
doi:10.1016/S0020-7683(03)00291-9

single simple shell structure to an integrated multi-shell structure (Prange and Schneider, 2001; Shin et al., 2002).

When the multi-shell structure is utilized, weight reduction can be easily realized because patches of plates can be added to different locations of the structure. During past decades, structural optimization has been popularized for weight reduction (Cassis and Schmit, 1976; Haug and Arora, 1979; Rangachargulu and Done, 1979; Schmit, 1981; Ashley, 1982; Vanderplaats, 1982; Hansen and Vanderplaats, 1990). In structural optimization, an objective function is minimized while various constraints are satisfied (Haftka and Gurdal, 1993). Each function should be mathematically defined. Structural optimization is classified into size, shape and topology designs according to the characteristics of the design variables (Haftka and Gurdal, 1993; Min et al., 1999; Barbarosie, 2003). They are quite efficient and sophisticated since they are mathematically well defined. However, the design problem should be defined to fit into the paradigm, which each technology pursues. Therefore, some other optimization methods such as fully stressed design (Hinton and Sienz, 1995; Mueller et al., 2002) and growth strain method (Han and Lim, 2002) have been developed as variances for mathematical optimization although they do not generate a mathematical optimum. These methods are fairly good in that they give moderate design solutions.

Design variables must be defined as specific optimization requires, when one of the above optimization technologies is adopted. Some applications of optimization have been performed for the automobile structures (Botkin, 2002; Shin et al., 2002). The researches show that the performance of a structure is improved. However, the design is carried out in a restricted sense to fit into the optimization paradigm. In practice, designers for the subframe want to define design variables in various manners and optimization is quite difficult and expensive with this freedom. Therefore, engineers design the subframe by using their intuition obtained from their experiences and many trial-and-error types of FE analyses although the application of optimization is not impossible. Design for weight reduction of the component often induces overly stressed weak regions. Entire redesign for stress-relieving of the weak region is, however, far from practical. If methods for supplementing the weak region of as-designed part are framed, a substantial amount of time and cost for redesign can be saved. Consequently, patches are often added to various weak locations of the subframe.

In this work, an automobile subframe is analyzed and redesigned. Finite element (FE) method is adopted for the analysis. The analysis results should be well incorporated into the design process. First, structural and load characteristics of the cross member and the #-type subframe model are analyzed via FE stress calculations. For a preset amount of stress relaxation in the weak region of the cross member, two local patching methods are proposed to help the practical design process. In the non-uniform method, the thickness of each shell element is separately designed to provide the final shape and thickness of patch. The concept is similar to that of the fully stressed design (Hinton and Sienz, 1995; Mueller et al., 2002) and growth method (Han and Lim, 2002). However, non-uniform thickness patching differs from them in that it keeps the original design shape. As a more practical way, the uniform thickness patching approach is also attempted. Certain areas are defined to have the same patching thickness. Conventional optimization algorithms are used to determine the areas and regression analysis is adopted for the approximation of the stresses to reduce computational time. We then present the axiomatic design approach to determine the optimal thickness of each subpart-shell in the integrated #-type subframe. The Independence Axiom of axiomatic design is adopted in this procedure (Suh, 1990, 2001). Functional requirements (FRs) are defined to relieve maximum stresses, and design parameters (DPs) are defined by a set of thickness of each panel. A design matrix is established from the investigation of the relation. It is found that the design matrix is a decoupled one. Therefore, the Independence Axiom is satisfied and the design sequence is defined as the design matrix indicates. At each step of the sequence, optimizations of the thickness of each panel are performed for weight reduction. These redesign approaches can be applied to other multi-shell structures such as the center member and the lower control arm.

2. Finite element stress analysis of multi-shell structures

2.1. Modeling of multi-shell structures

The boundary conditions for the cross member of the T-type subframe in a medium class passenger car are shown in Fig. 1. The upper part (E_c) of the cross member is loaded with engine inertia force which is transferred via the center member, and the lower part (B_c) is connected to the main body. The front (A_c) and rear (G_c) parts are connected to the control arm. The boundary conditions for the #-type subframe having higher crash resistance are shown in Fig. 2. The front (B_s) and rear (C_s) parts of the #-type subframe are connected to the main body. The middle (A_s) and end (G_s) parts are connected to the control arm. These front body frames are integrated multi-shell structures. The cross member consists of five subparts, while #-type subframe consists of eight subparts.

In contrast to the prior cross member made of a single part, the lightened new cross member consists of main body, and two connecting parts attached to both ends of main body (Fig. 3(a)). Each connecting part

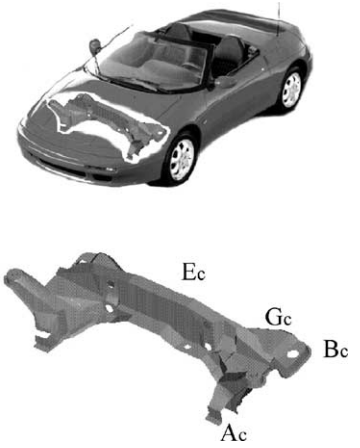

Fig. 1. Position and shape of cross member.

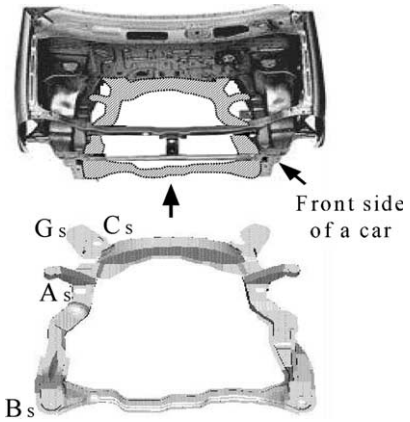

Fig. 2. Position and shape of subframe.

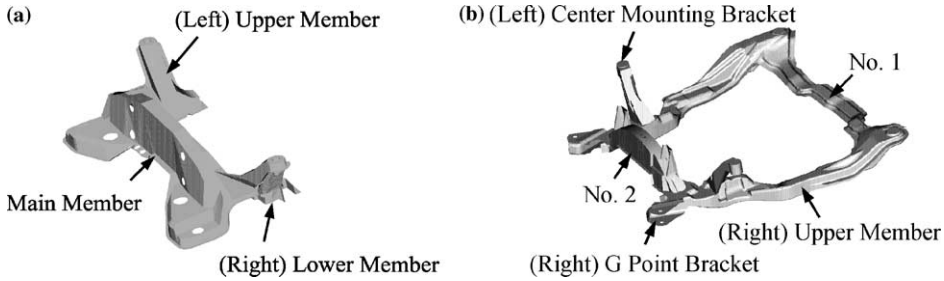

Fig. 3. (a) Shape of five parts of cross member. (b) Shape of eight parts of subframe.

consisting of upper and lower panels is connected to lower control arm. In short, the new cross member is a welding assembly of five subparts. Therefore, for more credible modeling, five subparts are modeled one by one. I-DEAS (1996) preprocessing program is used for FE modeling of cross member, and 4-node shell element (S4R: ABAQUS Library, 1998) is adopted. Then, we connect five subpart models at the weldment with 3-node shell element (STRIP3: ABAQUS Library, 1998) for proper modeling of seam weldment that connects each part continuously. Final FE model through these processes is shown in Fig. 4(a). The whole FE model consists of about 9200 elements of S4R and STRIP3, and about 9400 nodes. We then perform linear elastic analyses with the material SAPH41P, hot rolled high strength steel plate for automobile structure (Young's modulus $E = 200$ GPa, Poisson's ratio $v = 0.3$, yield strength $\sigma_y = 320$ MPa).

The integrated #-type subframe consists of total eight subparts, that is, No. 1, No. 2, (left and right) upper members, center mounting brackets and G-point brackets, as shown in Fig. 3(b). No. 1 connects with the front part of auto-body and its upper and lower panels are joined by spot welds. No. 2, left and right upper members respectively play the roles of cross and center members, which form the prior T-type subframe. Center mounting bracket and G-point bracket connects with suspension unit and lower control arm respectively so as to transfer driving load to auto-body. In short, integrated #-type subframe for medium class passenger car is also a welding assembly of eight subparts. Therefore, for more credible modeling, all parts are modeled separately, and 4-node shell element is used. FE models of subparts are joined at weldment using rigid beam element (MPC: ABAQUS User's Manual, 1998) for proper modeling of seam weldment connecting each part continuously. Final FE model formed through these processes is shown in Fig. 4(b). The whole FE model consists of about 34 000 S4R elements and about 36 700 nodes. We then perform linear elastic analyses with the material SAPH41P, hot rolled high strength steel plate for automobile structure (Young's modulus $E = 200$ GPa, Poisson's ratio $v = 0.3$, yield strength $\sigma_y = 277$ MPa).

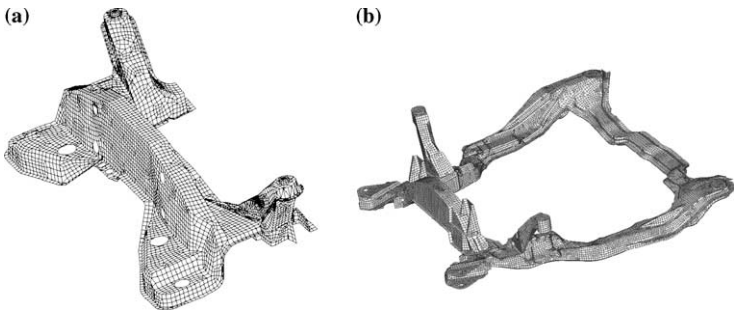

Fig. 4. FE models of (a) cross member, (b) subframe.

2.2. FE stress solutions of multi-shell structures

Boundary and load conditions applied to FE analyses of cross member and subframe are as follows. Since B_c, B_s and C_s parts are connected to the main body, relative displacements to body are zeroes. Therefore, we fixed the x-, y-, z-directional displacements and rotations of the fixture parts for connection. We also apply some driving loading conditions proposed by car manufacturers to D_c and D_s parts connected to suspension unit. Moreover, torque and load generated from engine during car driving are transferred to the engine mount in center member. Maximum transferred load measured by load cell attached just under the engine mount was 148 kgf. This maximum load can be converted into an approximate dynamic load, 296 kgf; the twice of static load. If we regard this dynamic load as a concentrated load, the load transferred to the cross member through joint area between center member and cross member is calculated as 48 kgf. The parts A_c, G_c and A_s, G_s are installed to lower control arm, and loading conditions at those parts depend on the driving conditions of front wheels. Our preliminary analyses revealed that, among various driving conditions, the sudden brake generates the most severe loadings on the parts A and G. Sudden brake condition is thus selected as the FE loading conditions for the cross member and the subframe. Those boundary and loading conditions under sudden brake are summarized in Fig. 5 and Table 1. FE stress solutions in the sudden brake loading conditions are shown in Fig. 6. We observe that the stress concentrates on the region a bit away from the front middle part of cross member as shown in Fig. 6(a). In this case, maximum stress (429 MPa) is 1.34 times the yield strength of SAPH41P (320 MPa). For the case of subframe, the stress concentrates on the left and right upper loading point connected to lower control arm as shown in Fig. 6(b). Maximum stress (314 MPa) is 1.13 times the yield strength of SAPH38P

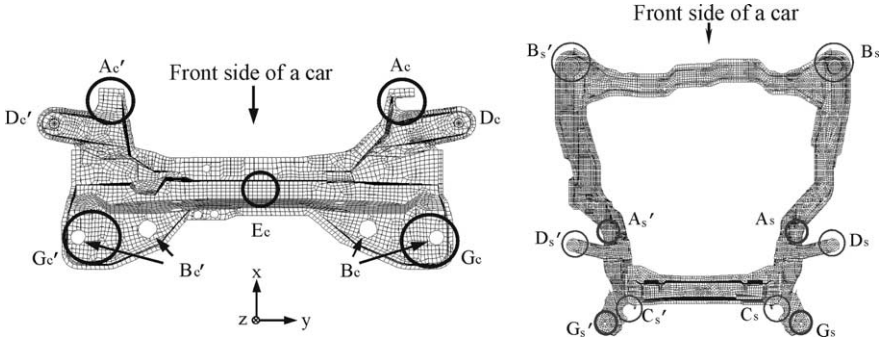

Fig. 5. Boundary conditions of (a) cross member, (b) subframe.

Table 1
Boundary and loading conditions of parts at sudden brake (see Fig. 5)

Parts	Boundary conditions	Loading conditions (kgf)						
Cross member	B_c, D_c (B_c', D_c')	$A_c(A_c')$			$G_c(G_c')$			E_c
		F_x	F_y	F_z	F_x	F_y	F_z	F_z
	All fixed	−645	1191	−82	−220	−978	−81	48
Subframe	B_s, C_s, D_s (B_s', C_s', D_s')	$A_s(A_s')$			$G_s(G_s')$			
		F_x	F_y	F_z	F_x	F_y	F_z	
	All fixed	−640	1191	−87	−220	−977	−81	

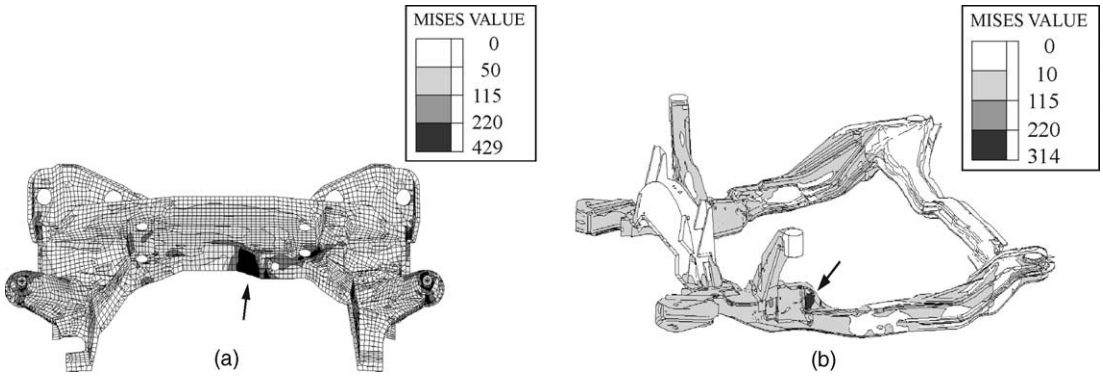

Fig. 6. Equivalent stress distribution of (a) cross member, (b) subframe at sudden brake.

(277 MPa). These stress solutions clearly suggest that certain measures need to be taken for stress relaxation in pre-designed cross member and subframe. Given the above pre-designed cross member model, we attempt to relax stress of weak region by non-uniform and uniform thickness patching methods. For the pre-designed #-type subframe model, to achieve both stress relaxation of weak region and weight reduction, we also present the axiomatic design approach of determining the optimal thickness of each subpart-shell.

3. Non-uniform thickness patching method

To reduce stress without changing a given shape of pre-designed cross member, we may consider patching up the weak region. As a way of determining the shape and thickness of patch, first, we increase the thickness of FE having maximum (equivalent) stress in stress concentrated region. The thickness in-

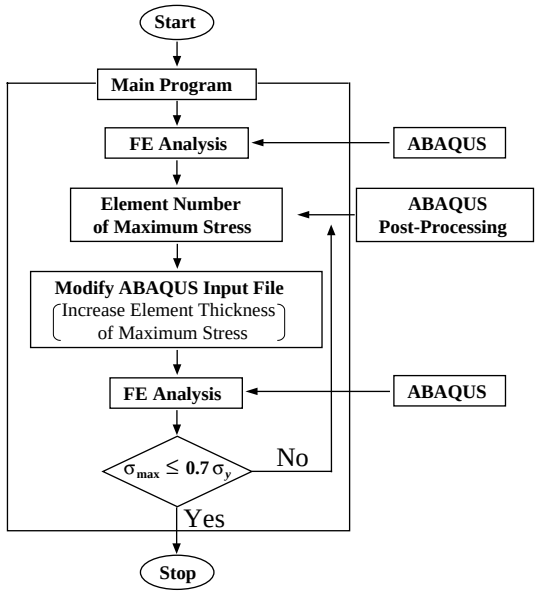

Fig. 7. Program flow-chart of increasing thickness for stress relaxation.

crease of that specific FE would bring about stress redistribution. Repeating the process would ultimately determine the shape and thickness of patch, which relaxes the maximum stress to a specific value. We attempt to relax the original maximum stress (429 MPa) down to 70% (225 MPa) of yield strength of SAPH41P (320 MPa). For each repetition, we increase the thickness of maximum-stressed FE by half of pre-designed thickness of the panel (= 2.3 mm). We prepared a program executing this repetition process. Fig. 7 shows the flow chart of "automatic thickness increasing FE analysis program". A proper shape and thickness of patch was reached after 90 repetition. Calculation was performed with HP C-Class workstation, and CPU time per step was 240 s. Stress distributions of stress concentrated region at intermediate 30, 60, 90th step, are zoomed up in Fig. 8. The followings are featured from the redistribution of equivalent stress at each step during repetition process. That is, in the middle of concentrated region where thickness barely varies, stress relaxes gradually, while in the bottom region where thickness increases directly, equivalent stress increases first and then decreases. This comes from an abrupt geometric change due to thickness increase. The final patch after 90th iteration has the varying thickness from FE to FE, and its shape is shown in Fig. 9. The patch weight is 0.10 kg, about 0.6% of the weight of whole cross member.

Usability of above method reduces by half in that the thickness varies from element to element which results in a non-uniform thickness patch. After all, from the practical point of view, a set of uniform thickness patch is needed to form a non-uniform thickness patch. In such case, the method requires experience and subjective decision of engineer. However, if an optimum set of uniform thickness patch for the

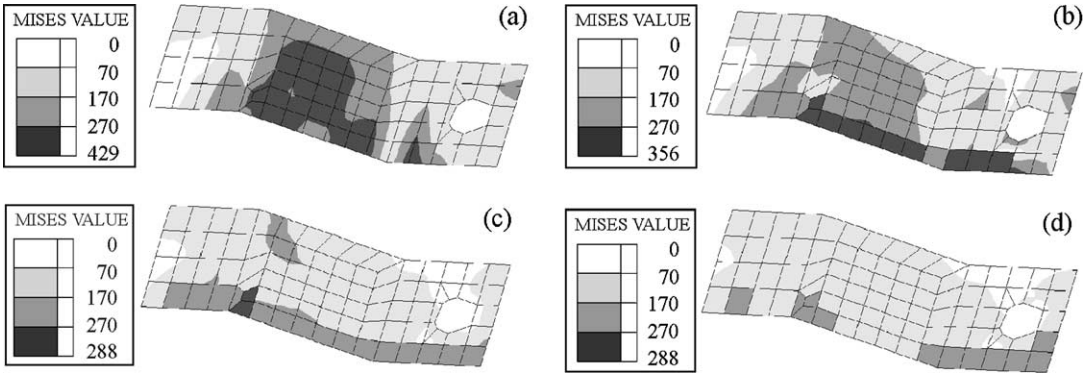

Fig. 8. Equivalent stress distributions of the stress concentration part. (a) Initial state (σ_{max}: 429 MPa). (b) State of step 30 (σ_{max}: 356 MPa). (c) State of step 60 (σ_{max}: 288 MPa). (d) State of step 90 (σ_{max}: 255 MPa).

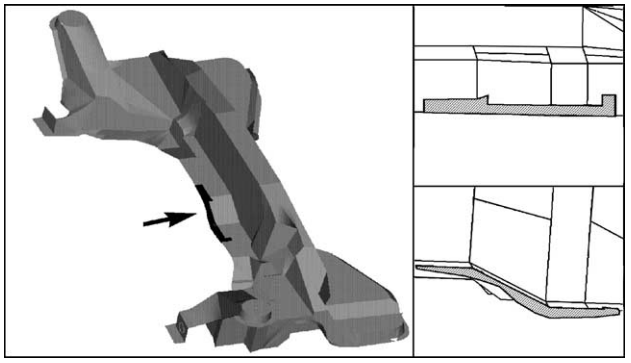

Fig. 9. Position and shape of an optimized non-uniform thickness patch.

configuration of non-uniform thickness patch can be determined systematically, usability of the gradual-thickness-increasing method will be doubled.

4. Uniform thickness patching method

4.1. FE analysis for uniform thickness patch

To overcome limitations of above gradual-thickness-increasing method which results in a non-uniform thickness patch, we present a uniform-thickness-patching method in this section, as another way for stress relaxation in the pre-designed cross member. We attempt to put a proper uniform thickness patch to the stress concentration region. The length and width of the region are about $l_0 = 112$ mm and width $w_0 = 56$ mm. First, to see the effect of length (l_p) and thickness (t_p) of patch on stress relaxation, with patch width (w_p) fixed as 56 mm, FE analyses are repeated for various values of l_p and t_p. Shown in Fig. 10(a) are maximum equivalent stresses at concentrated region from FE analyses for nine patch shapes with various values of l_p and t_p. In the figure, all parameters are normalized as $l = l_p/l_0$, $w = w_p/w_0$, $t = t_p/t_0$. It is observed that maximum stress is substantially affected with patch thickness, but barely affected with patch length. Therefore, if l_p is greater than minimum length covering stress concentration region, it no longer affect maximum stress at stress concentration region. Thus, the patch length is set as the minimum length; $l_p = l_0 = 112$ mm. To see the effect w_p of t_p and on stress relaxation, with fixed $l_p = 112$ mm, FE analyses are repeated for various values w_p of t_p and shown in Fig. 10(b) are maximum equivalent stresses at concentrated region from FE analyses for 12 patch shapes with various values w_p of t_p and it is observed that maximum stress is notably affected with w_p as well as t_p. This arises from deformation and loading characteristics of cross member under sudden brake such that bending moment is mainly applied to the section along patch width and thickness rather than to the section along patch length and thickness. Further, the marked effect of thickness on maximum stress is explained with the fact that stress induced by bending moment is inversely proportional to the square of thickness, while it is simply in inverse proportional to width. As the patch length has negligible effect on maximum stress as long as $l = l_p/l_0 \geqslant 1$, we select w_p and t_p as DPs, and optimize them. To begin with, we obtain the regression equation of equivalent stress by selecting five representative values of maximum stresses in patched cross member. All length parameters in equations below are normalized as $w = w_p/w_0$, $t = t_p/t_0$.

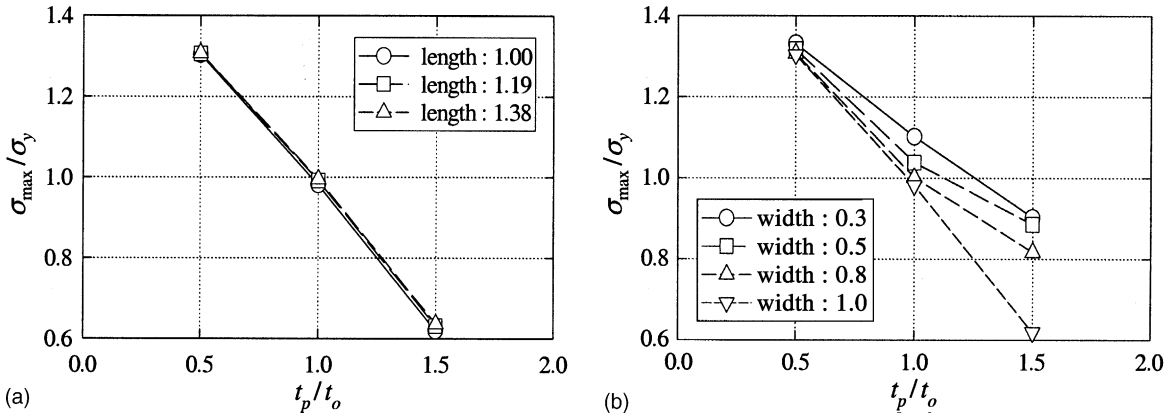

Fig. 10. Relations between maximum stress and thickness for (a) various lengths, (b) various widths.

4.2. Equivalent stress regression equation

Being in plane stress condition, stresses in cross member can be decomposed into three components; tension (σ_t), bending (σ_b) and torsion (τ) stresses. Taylor series approximations of these stress components provide following expression.

$$\sigma_t = \frac{F/A_0}{1 + A_p/A_0} = C_1'' + C_2''(-A_p/A_0) + C_3''(-A_p/A_0)^2, \tag{1}$$

$$\sigma_b = \frac{M_b r_0/I_{zz}}{1 + A_p r_0^2/I_{zz}} = C_4'' + C_5''(-A_p r_0^2/I_{zz}) + C_6''(A_p r_0^2/I_{zz})^2, \tag{2}$$

$$\tau = \frac{M_t r_0/I_z}{1 + A_p r_0^2/I_z} = C_7'' + C_8''(-A_p r_0^2/I_z) + C_9''(-A_p r_0^2/I_z)^2. \tag{3}$$

Here, F, M_b, and M_t denote force, bending and torsional moments at an arbitrary section normal to the longitudinal direction (y-direction in Fig. 5(a)) of cross member, and A_0, I_{zz}, and I_z denote area, second and polar moment of inertia of the section, respectively. A_p means sectional area of patch, and $C_i''(i = 1, 9)$ are undetermined constants. We now present the equivalent stress as

$$(\sigma_e/\sigma_y)^2 = [(C_{10}''\sigma_t + C_{11}''\sigma_b)^2 + C_{12}''\tau^2]/\sigma_y^2. \tag{4}$$

Substituting Eqs. (1)–(3) into Eq. (4) gives

$$(\sigma_e/\sigma_y)^2 = \sum_{i=0}^{4} C_i'(-A)^i. \tag{5}$$

Here the undetermined coefficients C_i' are proper sets of C_{ii}'', and the normalized sectional area A of patch is $A = \mathrm{lt}$, or $A = \mathrm{wt}$. Taking up to the second order term after replacing A with lt or wt, and arranging gives the following equation. Note that the patch length l is constant since it was fixed as its minimum.

$$(\sigma_e/\sigma_y)^2 = C_0 - C_1 t + C_2 t^2 - C_3 tw + C_4 t^2 w^2. \tag{6}$$

Replacing terms in Eq. (6) with the patch width, thickness and corresponding maximum equivalent stress values from FE analyses provides five simultaneous equations for five unknown constants. Solutions to the simultaneous equations obtained by LU decomposition method are $(C_0, C_1, C_2, C_3, C_4) = (2.85, 2.60, 0.853,$

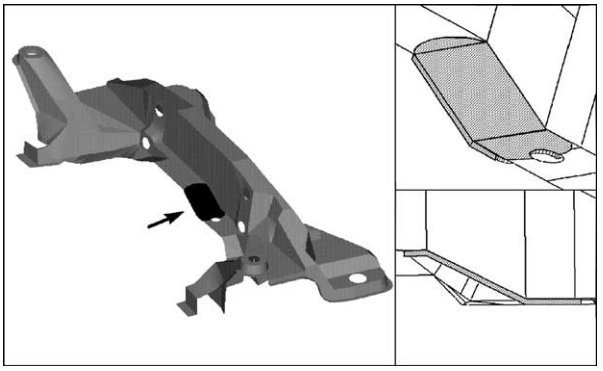

Fig. 11. Position and shape of an optimized uniform thickness patch.

Table 2
Maximum stress and shape of an optimized uniform thickness patch

Shape of optimized patch	Constraint of stress	FEM solution
$w = 1.0$ (56 mm) $t = 1.53$ (3.52 mm)	189 (MPa)	190 (MPa)

$-0.096, -0.279$). Average error of Eq. (6) compared to FE solution is 2% for 12 types of patch, which validates Eq. (6).

4.3. Optimized patching method

With weight reduction and stress relaxation given as primary targets, the weight of patch is selected as an object function, and constraint is selected so that maximum stress is less than 60% of yield strength. The volume of patch is the product of length, width and thickness, and then the weight is multiplication of volume by density. For fixed length and density, normalized object function of weight W is given as the product of normalized patch width by normalized panel thickness; $W(w,t) = wt$, where $w = w_p/w_0$, $t = t_p/t_0$. Moreover, if we let maximum stress be under 60% of yield strength for safety, we obtain the constraint equation as $\sigma_e \leqslant 0.6\ \sigma_y = 189$ MPa. We also put geometric constraint such that the patch width is less than the width of stress concentration region ($0 \leqslant w \leqslant 1$), and the patch thickness is less than three times of panel thickness ($0 \leqslant t \leqslant 3$).

A minimum patch satisfying the above constraints is obtained by using a commercial optimum design code, IDESIGN (Arora and Tseng, 1986). Fig. 11 presents the position and shape of an optimized uniform thickness patch. Table 2 shows that the width of optimum patch is determined as the value of upper limit, and thickness is determined as a proper value within the limit range. The fact that patch width reached to the given upper limit is related to the beam theory, which means that stress due to bending moment is inversely proportional to square of thickness, and is simply in inverse proportional to width. FE analysis of the cross member attached with the optimum patch provides the maximum equivalent stress of 190 MPa. This value differs only 0.5% from the design requirement (189 MPa). In summary, the optimized uniform thickness patch method is very practical in view of its relative ease of use and effectiveness.

4.4. Estimation of uniform thickness patching method

Maximum stress at stress concentration region without patching was 429 MPa, quite exceeding yield strength (320 MPa). An optimized uniform thickness patch has been obtained to relax this high stress state.

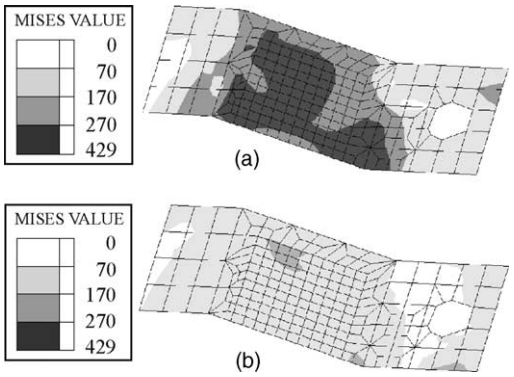

Fig. 12. Equivalent stress distributions (a) before patching, (b) after patching.

Maximum stress at stress concentration region after patching has decreased to 190 MPa, that is, a lower stress level corresponding to 60% of yield strength. In order to prevent another stress concentration, we made the final patch shape be elliptical at its both ends. The patch weight is 0.17 kg, about 1% of the weight of whole cross member. Fig. 12 compares the stress distributions without and with patching in the stress concentration region of cross member. In marked contrast to the stress concentration before patching, stress after patching shows a fairly relaxed and rather flat distribution.

5. Design enhancement by axiomatic approach

5.1. A brief of axiomatic design

The premise of axiomatic design is that there exists a fundamental set of principles that determines good design practice. Two axioms are proposed by noting the common phenomena shared by all cases. The first independence axiom states that independence of FRs characterizing functional needs must be maintained during the design process. The second information axiom states that, among all the designs that satisfy the first axiom, the one with minimum information content is the best. Here, the minimum information content means that the probability for success is the highest. From these two axioms, many theorems and corollaries are derived (Suh, 1990).

In the (axiomatic) design world, there are four domains as shown in Fig. 13: client, function, physics, and process. A set in the left domain is satisfied by choosing a proper set in the right domain. Customer requirements (CRs) are a set of ultimate objects of design. FRs are a minimum set of independent requirements to achieve CRs. FRs describe the design objects under constraints. Constraints represent the bounds on an acceptable solution. By definition, a constraint is different from FRs in that it needs not to be independent of other constraints and FRs. DPs are a set of physical embodiments for fulfilling FRs. Process variables (PVs) are manufacturing methods for realizing DPs. Design process is a inter-domain mapping operation. The design equation for the product design is expressed as

$$\{\mathrm{FR}\} = [\mathrm{DM}]\{\mathrm{DP}\} \leftrightarrow \mathrm{FR}_i = \sum_j \mathrm{DM}_{ij}\mathrm{DP}_j. \tag{7}$$

Here $\{\mathrm{FR}\}$ is the FR vector and $\{\mathrm{DP}\}$ is the DP vector, and [DM] is the design matrix. To satisfy independence axiom, design matrix should be diagonal, or (inverse) triangular. If [DM] is diagonal, a FR is satisfied independently by a DP. This design is defined as an uncoupled design. If [DM] is (inverse) triangular, independence of FRs can be assured by adjusting DPs in a particular order. This type of design is called a decoupled design.

Designers can propose several designs, which satisfy first axiom for a given set of FRs. Information axiom allows us to measure the design quality, thereby to select the best design. The information content is directly related to the probability of achieving the FR. Probability for success increases as information quantity for accomplishing the FR decreases. Conversely, infinite information is necessary if the probability

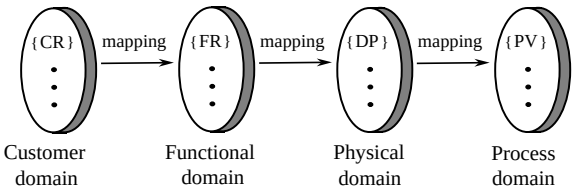

Fig. 13. Four domains of the design world.

for success approaches to zero. In short, information axiom means that the design with the minimum information content is the best one. In the next section, we apply this axiomatic approach to stress relaxation and weight reduction of #-type subframe.

5.2. Design of sub-frame through axiomatic approach

To relax stress of #-type subframe, FRs can be defined as follows.

FR1 = To relieve maximum stress of No. 1.
FR2 = To relieve maximum stress of No. 2.
FR3 = To relieve maximum stress of center mounting bracket (CMB).
FR4 = To relieve maximum stress of G-point bracket (GPB).
FR5 = To relieve maximum stress of upper member (UM).

It is observed that stress distributions in left and right sides of G-point bracket are at the same level, since the shapes of left and right sides of G-point are alike. Therefore, only "one" FR was allocated to the maximum stress for G-point. So were center mounting bracket and upper member. At the next stage of axiomatic approach, DPs satisfying those five FRs should be defined, and then optimum DPs satisfying given constraints should be determined. For this, we can first consider the shape of each subpart as a DP. However, shape optimization, being more complicated than parameter optimization, is not yet in the practical stage in spite of its well-established theoretical basis. Concretely, moving boundary condition due to shape change makes its application quite difficult. Algorithms for shape optimization are amply found in the literature, but the reliability, efficiency and accuracy of them seem to need further study (Kwak, 1994). To overcome the difficulty of shape optimization, Kim and Kim (1994) defined the shape of engine-mount with several shape parameters. They then determined the parameters so as to minimize the difference between design-specified stiffness and stiffness of shape defined by a set of shape parameters. Kwak et al. (1995) selected the patch thickness of auto-hood made of sheet molding compound (SMC) as a DP. They then designed a lightest SMC hood with the same stiffness of steel hood. As observed in those studies, defining subpart shape as a DP is inappropriate in terms of both information axiom and practical point of view. In this study, to satisfy FRs without changing subframe shape, we therefore define simple DPs as

DP1 = panel thickness of No. 1.
DP2 = panel thickness of No. 2.
DP3 = panel thickness of center mounting bracket (CMB).
DP4 = panel thickness of G-point bracket (GPB).
DP5 = panel thickness of upper member (UM).

The design using these FRs and DPs includes following three constraints.

Ct1: maximum stress is less than 80% of panel yield strength.
Ct2: $DP_i \geqslant 1$ mm for formability.
Ct3: weight of subframe is less than the as-pre-designed.

We first investigate the variation of stress at each subpart, when thickness of a specific part changes while thicknesses of the other subparts are fixed as the pre-designed values in Table 3. Fig. 14(a) and (b) are the two typical cases among those investigated. Fig. 14(a) shows the maximum stress variations of each subpart when thickness of only No. 2 changes. Fig. 14(b) shows the maximum stress variations of each subpart when thickness of only UM changes. Changed thickness t_p of a specific subpart is normalized with the

Table 3
Original thickness of each part

Parts	No. 1	No. 2	CM bracket	GP bracket	Upper member
Thickness (mm)	2.3	2.0	2.0	2.6	2.3

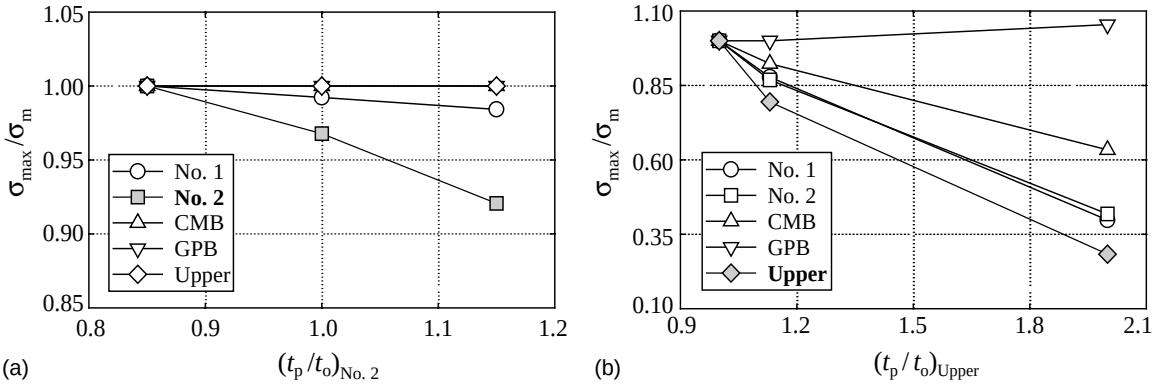

Fig. 14. Variation of maximum stress in each part for changes of thickness of (a) No. 2, (b) UM.

original thickness t_0 of that specific subpart. Maximum stress σ_{max} of each subpart is normalized with a maximum stress σ_m of that subpart (No. 1, No. 2, CMB, GPB, UM) obtained when thickness of a specific part (No. 2 in Fig. 14(a); UM in Fig. 14(b)) has the minimum value. We observe in Fig. 14(a) that for the thickness change of No. 2, only No. 2 itself shows notable variation in σ_{max}, while other subparts show insignificant variations. In short, thickness of No. 2 affects only σ_{max} of No. 2. The thickness of No. 1 was also observed to affect only σ_{max} of No. 1. So were CMB and GPB. On the other hand, when thickness of UM increases, σ_{max} of all subparts decreases except GPB as shown in Fig. 14(b). This is because UM plays the role of translating driving loads from lower control arm to other subparts. GPB, however, receives loads directly from lower control arm, which results in slight variation of σ_{max} in GPB even with thickness change of UM. Design matrix of Eq. (7) based on these observations comes to an inverse triangular matrix like Eq. (8).

$$\begin{pmatrix} \mathrm{FR1} \\ \mathrm{FR2} \\ \mathrm{FR3} \\ \mathrm{FR4} \\ \mathrm{FR5} \end{pmatrix} = \begin{bmatrix} X & O & O & O & X \\ O & X & O & O & X \\ O & O & X & O & X \\ O & O & O & X & O \\ O & O & O & O & X \end{bmatrix} \begin{pmatrix} \mathrm{DP1} \\ \mathrm{DP2} \\ \mathrm{DP3} \\ \mathrm{DP4} \\ \mathrm{DP5} \end{pmatrix}. \tag{8}$$

Here X and O mean that DP do and do not affect FR, respectively. In a rather complicated design with many FRs and DPs such as Eq. (8), investigation of sensitivity of FR with respect to each DP is the most essential work. This is because design matrix fixes the sequence for determining the optimum values of DPs. To determine DPs satisfying FRs in a design equation having inverse triangular matrix like Eq. (8), each DP should be defined one by one in reverse order, that is, from DP5 to DP1. In the previous section, concept of equivalent stress regression as Eq. (6) was introduced by Taylor series approximation of each stress component in terms of panel thickness and width. In this section, we determine optimum panel thickness satisfying Ct1 via simpler second order equation as follows.

$$C_0 + C_1 t + C_2 t^2 = \sigma_{max}/\sigma_y. \tag{9}$$

Table 4
Thickness and maximum stress of each subframe model

Parts	Model subframe		Optimized part thickness model	
	Thickness (mm)	Maximum stress (MPa)	Thickness (mm)	Maximum stress (MPa)
No. 1	2.3	64	1.0	59
No. 2	2.0	71	1.0	43
CMB	2.0	146	1.2	216
GPB	2.6	129	2.0	224
UM	2.3	314	2.8	224

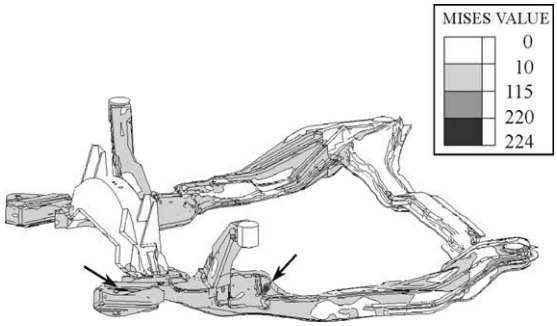

Fig. 15. Equivalent stress distribution in the subframe model with optimized part thicknesses at sudden brake.

Here $t = t_p/t_0$ (= ratio of changed thickness to original thickness of a specific subpart), σ_{max} is maximum stress at the specific subpart, σ_y is yield strength, and C_0, C_1, C_2 are unknown constants. To determine these constants in Eq. (9), three σ_{max} values for three thickness values of the specific subpart are needed. Values of σ_{max} are obtained by FE analyses for three different values of thickness of that subpart. By substituting three values of thickness and corresponding three values of σ_{max} into Eq. (9), three simultaneous equations for unknown constants C_0, C_1, C_2 are obtained. Solutions to the simultaneous equations obtained by LU decomposition method are $(C_0, C_1, C_2) = (3.24, -2.85, 0.71)$. When maximum stress of UM is 80% of yield strength, Eq. (9) then gives $t_p|_{Upper} = 1.23\ t_0|_{Upper} = 1.23 \times 2.3 = 2.8$ mm. FE analysis with $t_p|_{Upper} =$ 2.8 mm gives maximum stress of subframe as 224 MPa. This differs only 1% from 222 MPa (= 80% of yield strength of SAPH38P, which validates the approach by Eq. (9). Determining DP4-DP1 in the same manner, we obtain the thickness of each subpart as summarized in Table 4. When thickness of a specific subpart was varied with thicknesses of other subparts fixed, it was observed that maximum stress at No. 1 and No. 2 were always much lower than yield strength. Therefore, minimum thickness (1 mm) allowed for formability is selected as optimum thickness of No. 1 and No. 2. Fig. 15 shows the equivalent stress distribution by FE analysis at a sudden brake condition for #-type subframe model consisting of optimum thicknesses of subparts. Table 4 also shows the flatted stress distribution that is an indication of enhanced structural efficiency.

6. Summary

In this work, we first developed an "automatic thickness increasing FE analysis program" (Fig. 7). This program locates the FE with maximum stress. Thickness increase of that specific FE yields stress redistribution. Progressive local thickness increase finally determines the shape of patch with non-uniform

Table 5
Weight and maximum effective stress for each patching type

Patching type	Weight (kg)	Maximum stress (MPa)	Ratio of stress (σ_{max}/σ_y)
Model cross member	16.10	429	1.36
Non-uniform thickness patch	16.20	225	0.70
Uniform thickness patch	16.27	190	0.60

Table 6
Weight and maximum stress for each sub-frame model

Model type	Weight (kg)	Maximum stress (MPa)	Ratio of stress (σ_{max}/σ_y)
Model subframe	24.15	314	1.13
Subframe model with optimized part thicknesses	20.23	224	0.81

thickness. The concept of equivalent stress regression Eq. (6) was then introduced for optimization of patch with uniform thickness. Both non-uniform thickness and optimized uniform thickness patches successfully bring preset amounts of stress relaxation in a pre-designed cross member. The latter is discussed to be more effective and practical. Axiomatic design method was applied to determine the thicknesses of subparts in a #-type subframe. Simpler second order interpolation equation (Eq. (6)) was introduced.

Table 5 compares the weight, maximum stress and stress ratio of as-pre-designed and patched cross members. Stress ratio is the ratio of maximum stress to yield strength of SAPH41P (320 MPa). It is noteworthy that maximum stress reduced considerably with negligible increase of weight. Table 6 compares the weight and maximum stress of as-pre-designed #-type subframe and the one with optimized subpart thicknesses. Subframe with optimized subpart thicknesses accurately decreases maximum stress to the preset value ($=0.8\sigma_y$). Stress ratio is the ratio of maximum stress to yield strength of SAPH38P (277 MPa). It is noteworthy that enhanced subframe model also gives the weight reduction effect of about 3.92 kg (16%). Manufacturer had relaxed the maximum stress to the same level ($=0.8\sigma_y$) with an experience-based patch of 3.89 kg. Compared with this patched one, enhanced subframe model gives a significant weight reduction effect of 7.81 kg (28%). The stress relaxation methods presented in this work can be applied to the other multi-shell structures such as center member and lower control arm.

References

ABAQUS User's Manual, 1998. Version 5.8, Hibbitt, Karlsson and Sorensen, Inc., Pawtucket, RI.

Ambrosio, J.A.C., 2003. Contact and impact models for vehicle crashworthiness simulation. International Journal of Crashworthiness 8 (1), 73–86.

Arora, J.S., Tseng, C.H., 1986. IDESIGNUser's Manual. Version 3.5, The University of Iowa, Iowa City, Iowa.

Ashley, H., 1982. On making things the best-Aeronautical uses of optimization. Journal of Aircraft 19 (21), 5–28.

Barbarosie, C., 2003. Shape optimization of periodic structures. Computational Mechanics 30 (3), 235–246.

Botkin, M.E., 2002. Structural Optimization of automotive body components based on parametric solid modeling. Engineering with Computers 18 (2), 109–115.

Cassis, J.H., Schmit, L.A., 1976. Optimum structural design with dynamic constraints. ASCE Journal of Structural Division ST10, 2053–2071.

Haftka, R.T., Gurdal, Z., 1993. Elements of Structural Optimization. Kluwer Academic Publishers, Dordrecht, The Netherlands.

Han, S.Y., Lim, J.K., 2002. Shape optimization for prolonging fatigue fife. JSME International Journal Series A—Solid Mechanics and Material Engineering 45 (2), 298–304.

Hansen, S.R., Vanderplaats, G.N., 1990. Approximation method for configuration optimization of trusses. AIAA Journal 28 (1), 161–168.

Haug, E.J., Arora, J.S., 1979. Applied Optimal Design. John Wiley and Son, New York, New York.
Hinton, E., Sienz, J., 1995. Fully stressed topological design of structures using an evolutionary approach. Engineering Computations 12, 229–244.
Hong, U.P., Park, G.J., 2003. Determination of the crash pulse and optimization of the crash components using the response surface approximate optimization. In: Proceedings of the Institution of Mechanical Engineers Part D—Journal of Automobile Engineering, vol. 217 (D3), pp. 203–213.
I-DEAS Master Series 3, 1996. Student Guide (P-30002), Structural Dynamics Research Corporation, Milford, OH.
Kim, J.-J., Kim, H.-Y., 1994. Shape Optimization of rubber for engine mount using shape parameter method. Korean Society of Automobile Engineering, vol. 2 (2), SAE No. 943715, pp. 33–41.
Kwak, B.M., 1994. A review on shape optimal design and sensitivity analysis. Structural Engineering/Earthquake Engineering 10 (4), 159s–174s.
Kwak, D.-Y., Chun, J.-S., Lim, Y.-T., 1995. Optimum design of SMC hood patch via stiffness analysis. In: Proceedings of KSME Autumn Conference (I), pp. 985–990.
Lam, L.T., 2003. Factors associated with fatal and injurious car crash among learner drivers in New South Wales, Australia. Accident Analysis and Prevention 35 (3), 333–340.
Min, S., Kikuchi, N., Park, Y.C., Kim, S., Chang, S., 1999. Optimal topology design of structures under dynamic loads. Structural Optimization 17 (2–3), 208–218.
Mueller, K.M., Liu, M., Burns, S.A., 2002. Fully stressed design of frame structures and multiple load paths. Journal of Structural Engineering-ASCE 128 (6), 806–814.
Prange, W., Schneider, C., 2001. Automobile light construction initiatives by the international steel industry. Stahl Und Eisen 121 (7), 23–29.
Rangachargulu, M.A.V., Done, G.T.S., 1979. A survey of structural design under dynamic constraints, shock and vibration. Digest 11 (12), 15–25.
Schmit, L.A., 1981. Structural synthesis—Its genesis and development. AIAA Journal 19 (10), 1249–1263.
Shin, J.K., Lee, K.H., Song, S.I., Park, G.J., 2002. Automotive door design with the ULSAB concept using structural optimization. Structural and Multidisciplinary Optimization 23 (4), 320–327.
Suh, N.P., 1990. The Principles of Design. Oxford University Press, New York (Chapter 2–3).
Suh, N.P., 2001. Axiomatic Design. Oxford University Press, New York.
Vanderplaats, G.N., 1982. Structural optimization—past, present, and future. AIAA Journal 20 (7), 992–1000.